FERMILAB-FN-1118-CMS-E

Induced Current Detector Simulation

Fermilab Note FN-1118-CMS-E

Ronald Lipton

Fermilab, PO Box 500, Batavia, Il 60510

Abstract

We describe simulations of a detector concept with small, low capacitance, pixels with pitch/thickness ratio on the order of 10. The simulation utilizes 2D and 3D TCAD simulations followed by a generic SPICE front-end model including noise and Landau fluctuations. We also investigate the properties of weighting fields of various geometries. We investigate whether the transient induced current signals can be used to improve pattern recognition and establish track angle.

Keywords: 3D Integration, Pixel Detector, Induced Currents, X-ray Imaging

1. Introduction

We describe a simulation of detectors based on induced current pulse shapes intended to estimate the timing, pattern recognition and angular discrimanation capabilities of these devices. The usual charge-integrating detectors ignore much of the information inherent in the complex pulse shapes in both charge-collecting and neighbor pixels. We investigate the characteristics of these pulses and estimate the utility of this information based on practical limits of noise, time resolution, signal complexity, and power. We also describe in some detail the characteristics of the weighting fields to provide some insight into the systematics of the resulting pulse shapes.

*Corresponding author
Email address: lipton@fnal.gov (Ronald Lipton)

This manuscript has been authored by Fermi Research Alliance, LLC under Contract No. DE-AC02-07CH11359 with the U.S. Department of Energy, Office of Science, Office of High Energy Physics.

2. Simulation Framework

We utilize a simulation chain that includes charge motion within the sensor and subsequent electronics response. Minimum Ionizing Particles (MIPs) are simulated by depositing MIP charges in a Technology Computer-Aided Design (TCAD) model of the detector. This information is passed to the electronics simulation. The chain includes:

- Generation of a sensor TCAD model
- Generation of a MIP current pulse library with varying track angles.
- Monte Carlo simulation of the resulting transient signals including amplifier noise and Landau fluctuations of the total pulse amplitude with a SPICE model of the detector and front-end amplifier
- Evaluation of the resulting time and angular resolutions

The TCAD model of the sensor is parametrized as a function of sensor thickness and pixel geometry. We do not Monte Carlo the Landau fluctuations in the detector currents. As a result the actual input pulse shape does not vary. Inclusion of effects such as fluctuations in charge deposit and delta rays are not practical in the TCAD environment, as the finite element grid in the TCAD introduces discretization effects comparable to the charge deposit fluctuations. In the absence of a full front-end amplifier design we approximate the amplifier noise response by a parametrized SPICE simulation. Time resolutions are measured by a Monte Carlo-based transient analysis with fixed thresholds.

3. Amplifier Simulation

We simulate the front-end amplifier as a generic amplifier configured as a transimpedance amplifier with feedback resistor (figure 1). B1 is the voltage noise source and B2 the current noise source. I1 is the electrode current signal imported from the TCAD model. In our case the amplifier, U1, is modeled with

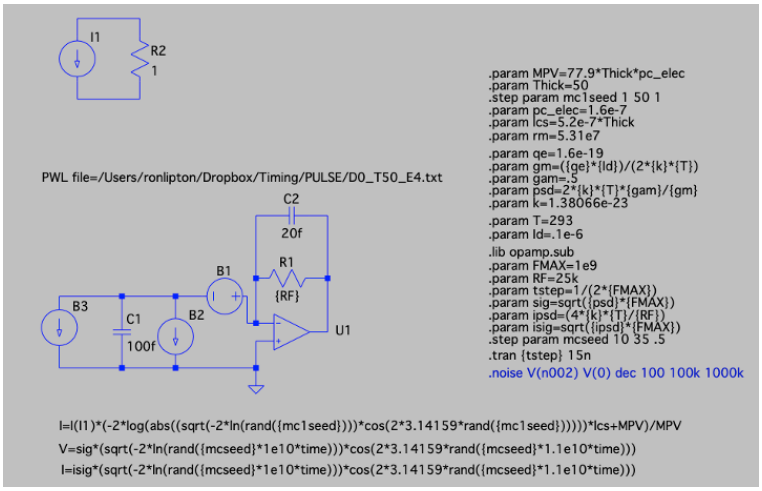

Figure 1: Transimpedance amplifier with current and voltage noise sources used for transient simulation.

a gain-bandwidth of 500 MHz and transductence set by the input transistor drain current parameter, I_d.

The noise is related to the input transistor and circuit design. We assume front-end transistor operation in weak inversion for the relation between transductence and drain current. The power spectral densities for voltage (e_n) and current (i_n) white noise are:

$$e_n^2 = \frac{2kT\gamma}{g_m}, i_n^2 = \frac{4kT}{R_F}, g_m = \frac{q_e \times I_d}{2kT} \tag{1}$$

Where g_m is the input transistor transductance, q_e is the electron charge, k is the Boltzmann constant, and T is the temperature. White noise is simulated in the time domain as in reference [1] :

$$n(t) = \sigma_n \times \eta(t, \delta t), \delta t = \frac{1}{2F_{max}}, \sigma_n = \sqrt{e_n^2, i_n^2 \times F_{max}} \tag{2}$$

Where $n(t)$ is the white noise signal, σ_n is the current or voltage white noise derived from the spectral power densities, F_{max} is the maximum frequency, and η is a Gaussian distributed random number updated with the interval δt. Landau fluctuations in the signal amplitude are added by utilizing a current-controlled

behavioral source (B3) including the amplitude fluctuations. Additional references on transient noise simulation in SPICE are available in [2][3][4][5][6].

4. Weighting Fields

Motion of charge in an a multi-electrode detector results in a distribution of currents on the electrodes. These currents can be calculated using the Shockley-Ramo theorm[7][8]. The shape and magnitude of the currents depends both on the "weighting field" which quantifies the coupling to each electrode, and the charge velocity, $i = E_w q v$. The weighting field, E_w, is calculated by setting the electrode of interest to 1V and grounding the other electrodes. TCAD programs perform this analysis automatically as part of their solution of the equations of motion in the semiconductor. The current induced on an electrode depends directly on the weighting field of that electrode at the position of the moving charge. The weighting field value will in turn depend on the geometry of the sensor and the size of the electrode.

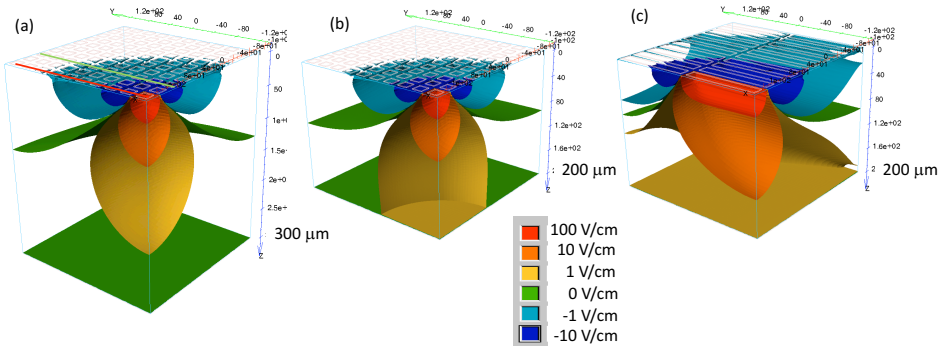

Figure 2: 3D weighting field simulation of a 10x10 array of pixels on 25 micron pitch with 300 (a) and 200 (b) micron thickness and a 2 x 10 array (c) on a 200 micron substate with 125 x 25 micron pitch. Constant weighting field contours at -10, -1, 0, 1, 10, and 100 V/cm are shown

To demonstrate these effects we produced a three-dimensional simulation with variable values of pixel dimension and detector thickness. The weighting field is calculated by replacing the silicon substrate by a SiO_2 and biasing the "home" electrode to 1V. Figure 2 shows equal weighting field profiles for a 10x10 pixel array on 25 micron pitch for detectors of 300 and 200 micron thickness as well as a 2 x 10 array with 125 x 25 micron pitch. All have the home pixel at the near right. The green surface at E=0 represents the location where the weighting field changes from positive to negative. Reducing the thickness of the 25 x 25 micron pixel arrays from 300 to 200 microns is equivalent to removing the bottom 100 microns of the thicker substrate. Increasing the size of the pixels in one dimension as in figure 2c significantly extends the high field region. This will also increase the resulting signal current in neighboring pixels. For this reason 2D simulations significantly underestimate the induced current in square arrays of small pixels. For applications such as tracking where resolution in one dimension may be more important than the other there may be benefit to rectangular pixels despite the larger load capacitance. In this simulation field shapes near the edges of the modeled region are distorted by the Neumann (reflective) boundary conditions used by the simulation. Accurate modeling of a local region requires that the region be far from an edge and the model transverse dimensions be larger than the device thickness.

Charge motion in the weighting field will induce a current in the home pixel proportional to the integral of currents times the local weighting field. Figures 3a and b show slices of the 3D sensor simulation at x=-112.5 (red line) and -62.5 microns (green line), the centers of the near and third pixel rows. In these projections the scales are logarithmic. If we consider tracks with normal incidence, the weighting field corresponding to the home pixel (X=-112.5, Y=-112.5) is positive, corresponding to unipolar induced current. As we move away from the home pixel the region where the weighting field changes sign can be seen as the valley between two lobes. This is clear in 3b where the home pixel will collect zero total charge in all cases. In these detectors, with large thickness to pitch ratios, the large region where the depth is large compared to home

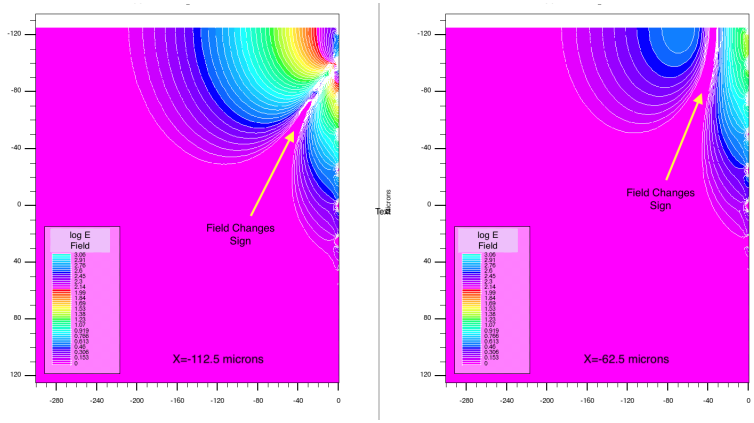

Figure 3: (a) and (b) are slices of of the structure in figure at X=-112 (red line) and -62.5 (green line) microns. The contours are shown on a log scale. Also indicated is the region ($E_w = 0$) where the field changes sign.

pixel dimensions has positive weighting field, while the regions close to the electrodes have larger, negative weighting fields. As can be seen in the next section, understanding the weighting field geometry is crucial in understanding the resulting current pulses.

5. Sensor Current Pulse Characteristics

For a detector where the electrode pitch is small compared to the thickness, charge deposited far from the surface will induce current pulses on a number of surrounding electrodes. For those electrodes that do not collect charge the current signals are bipolar and the current sums to zero. The induced signals can have a very fast rise time and characteristic shapes that can be used both for fast timing and for track angle measurement. An example is shown in figure 4, where charge is deposited 190-195 microns deep in a 200 micron thick detector with 25 micron electrode spacing. The central electrode (brown) collects most of the charge, with the neighbor collecting about 15%. The other electrodes sum to zero. All electrodes have an induced current immediately after charge motion begins ranging from a peak current of 14% of the maximum current

on the central electrode to 2% for the electrode 200 microns away from the central electrode. For track-like deposits this picture changes as the positive and negative induced currents can cancel near t=0 and slow the effective rise time.

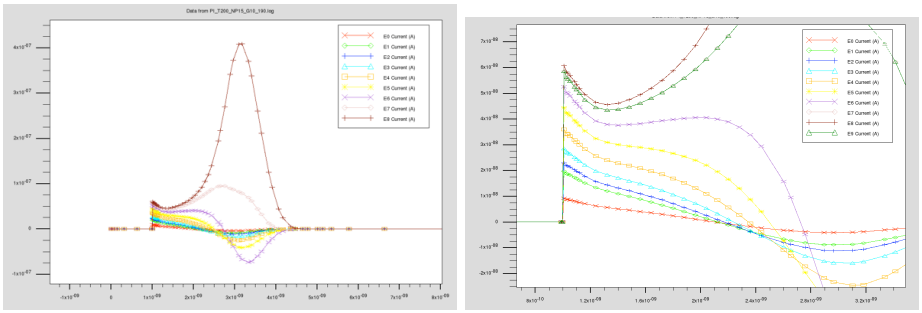

Figure 4: Current pulses in a 2D multi-electrode detector with charge deposited at a depth of 190-195 microns

The simulations in figure 4 demonstrate the fall in induced current as a function of distance from the central pixel. Figure 5 shows the size of the initial induced current spike as a function of the pixel distance from a charge deposit 190-195 microns deep in a 200 micron thick detector. This is effectively a measure of the weighting field at y 190 microns. These are 2D simulations. In three dimensions the effective value of the weighting field falls with pixel size.

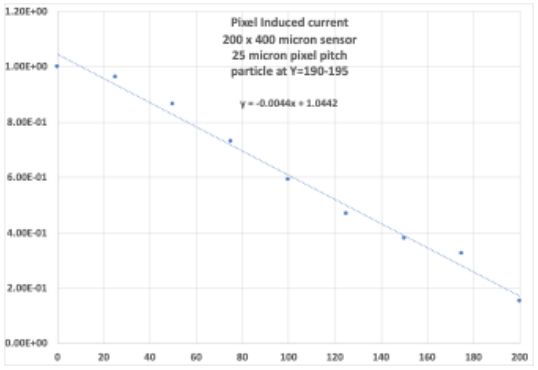

Figure 5: 2D pixel current normalized to the central pixel as a function of pixel x distance from charge deposited at a depth (y) of 190-195 microns

To compare 2D and 3D simulations, we performed a full 3D simulation of a 5x5, 200 micron thick, 25 micron pitch array. Shown in figure 6 is the 3D model showing the current due to a track with incident angle of 8 degrees after 200ps. The cutline is at y=0. To compare the 2D and 3D simulations approximate the 2D situation by adding the signals from a y row of pixels in the 3D simulation.

The resulting pulses are shown in figure 7 which compares pulse shapes from individual pixels and summed rows for 0 and 8 degree tracks. The normalization between (a) and (b) is arbitrary due to the dependent of the TCAD charge deposit on the orientation of the finite element grid. The zero degree track is dominated by the pulse in the central electrode with a fast rise due to charge motion near the electrode. The neighbor pixels and rows have a slower rise time, with the slow component dominated by hole drift to the cathode. The fast rise seen in figure 4 for deep local charge deposition is now much slower due to integration of initial charge motion contributions contributing positive and negative components through the depth of the detector. For the 8 degree track the central electrode still has the dominant signal but now the charge deposited near the neighbor electrode also provides a large, fast rise initial signal. Individual neighbor pixels again provide small, slow signals. However the sum of the row in y provides a signal of significant size due to the larger integral weighting field. For applications where one dimension is preferred, such as a track trigger filter similar to the CMS two-layer modules, a 2D design provides better signal/noise. It is also appealing to consider a readout strategy with current value samples at t=0 (one ns in figure 7) followed by sample at one to two ns intervals.

6. Analysis and Angular Reconstruction

The internal motion of currents in a detector present a complex set of pulse shapes in each event that depend on the distribution of these currents within the detector. For our initial study we assume a model for each pixel which includes a front-end amplifier model as described in section 3, figure 1. We also assume

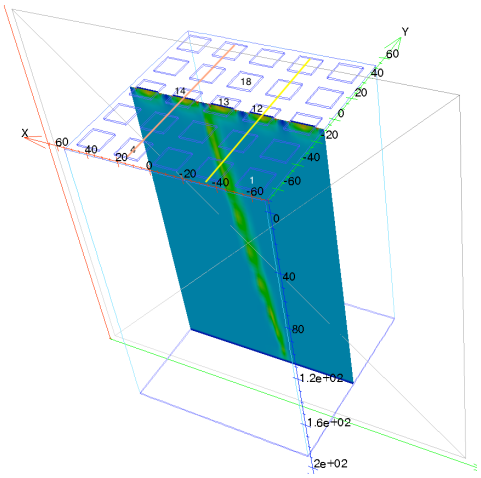

Figure 6: Pixel array with pitch of 25 microns and detector thickness of 200 microns with a track injected at 8 degree incidence. The cutline at y=0 shows the total conduction current at 200 ps after carrier injection. Pixel numbers correspond to pulse labels in figure 7

.

a three-level discriminator system which includes time-over threshold for the three levels. Figure 8 shows an example for a neighbor electrode (electrode 5) with a 0 degree track incident on electrode 4.

Figure 9 shows the distributions of T and ΔT for tracks passing through the detector centered on electrode 4. There is a clear difference between the 0 and 4 degree pattern. At normal incidence only the lower threshold is triggered for the neighbor pixels and the start times are closely clustered. At four degrees seven pixels are triggered at the lowest threshold, five at the intermediate value, and two at the high threshold. The distributions of start times and delta times also provide indications of the sign of the angle.

These points represent the centroid values of the times, and do not include Landau fluctuations. These patterns are complex, especially if we include variations of track locations with respect to the center of the pixel array. It should not be difficult to distinguish between large and small angle tracks, but how much detailed information can be extracted on-pixel will depend on the sophistication of the algorithms that can be integrated into the chips. This data is

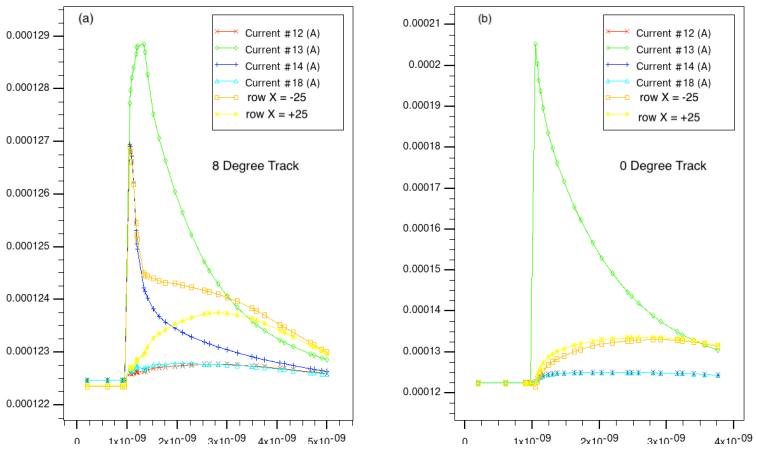

Figure 7: Individual electrode pulses in the central electrode (13) and it's neighbors as well as the pulse formed by adding the pixels at x=25 (orange) and x=-25 (yellow) microns. Electrode numbers refer to the labels in figure 6.

from a 2D simulation. For a 2D pixel array the signal will be reduced by weighting field effects, discussed in section 4. This will modify the pattern of pixels above threshold.

An alternate technique would be to use a moderately high threshold for a seed pixel and then latch neighbor pixel pulse values at t=0 and additional fixed delta T values. This reduces the overall power by eliminating discriminator switching and allows for crude waveform analysis.

7. Conclusions

Newly available capabilities with fast, low power, amplifiers and fine segmentation of detector elements allow us to utilize ns-level characteristics of pulse shapes in silicon detectors. This can, in turn, allow fast timing, background rejection in noisy environments, and selection of incident track charactoristics. We have described a process to simulate signal generation and amplifier response and noise using standard TCAD tools and generic SPICE models. This allows for a qualitative understanding of the design of a detector system without

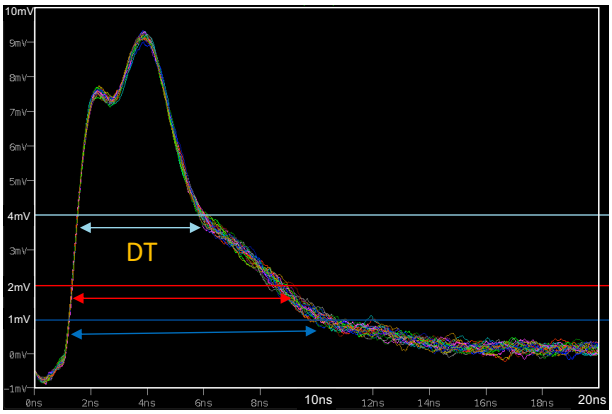

Figure 8: Example current pulse with three discriminator thresholds.

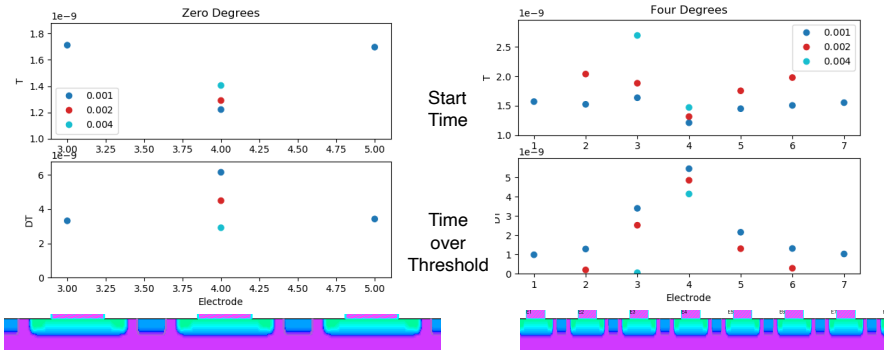

Figure 9: Distribution of hit time and time over threshold for tracks a 0 degree (left) and 4 degree incidence

detailed IC design simulations. Three dimensional weighting field simulations were performed as an aid in understanding field effects on the electrode pulses as a function of detector geometry and thickness. As an example we then showed how track angles can be reconstructed with small pixels including a 3-level discriminator system.

8. Acknowledgments

This manuscript has been authored by Fermi Research Alliance, LLC under Contract No. DE-AC02-07CH11359 with the U.S. Department of Energy, Office of Science, Office of High Energy Physics.

9. References

References

[1] Cadence, Application notes on direct time-domain noise analysis using virtuoso spectre, Tech. rep.

[2] S. C. Terry, B. J. Blalock, J. M. Rochelle, M. N. Ericson, S. D. Caylor, Time-domain noise analysis of linear time-invariant and linear time-variant systems using matlab and hspice, IEEE Transactions on Nuclear Science 52 (3) (2005) 805–812.

[3] A. Pullia, S. Riboldi, Time-domain simulation of electronic noises, IEEE Transactions on Nuclear Science 51 (4) (2004) 1817–1823.

[4] R. H. Redus, A. C. Huber, Monte carlo time domain noise simulation in nuclear electronics, in: 2008 IEEE Nuclear Science Symposium Conference Record, 2008, pp. 3421–3429.

[5] T.-H. Lee, G. Cho, Monte carlo based time-domain hspice noise simulation for csa-crrc circuit, Nuclear Instruments and Methods in Physics Research Section A: Accelerators, Spectrometers, Detectors and Associated Equipment 505 (1) (2003) 328 – 333, proceedings of the tenth Symposium on Radiation Measurements and Applications. doi:https://doi.org/10.1016/S0168-9002(03)01090-8.
URL http://www.sciencedirect.com/science/article/pii/S0168900203010908

[6] P. O'Connor, G. D. Geronimo], Prospects for charge sensitive amplifiers in scaled cmos, Nuclear Instruments and Methods in Physics Research Section A: Accelerators, Spectrometers, Detectors and Associated Equipment 480 (2) (2002) 713 – 725. doi:https://doi.org/10.1016/S0168-9002(01)01212-8.
URL http://www.sciencedirect.com/science/article/pii/S0168900201012128

[7] W. Shockley, Currents to conductors induced by a moving point charge, Journal of Applied Physics 9 (10) (1938) 635.

[8] S. Ramo, Currents induced by electron motion, Proceedings of the IRE 27 (8) (1939) 584–585.